forests

MDPI

Article

# Quantitative Spatiotemporal Oil Body Ultrastructure Helps to Verify the Distinct Lipid Deposition Patterns in Benzoin Endosperm and Embryo Cells

**Zihan Zhang [1], Ying Luo [1,2], Xiaojun Wang [1] and Fangyuan Yu [2,*]**

[1] Collaborative Innovation Center of Sustainable Forestry in Southern China, College of Forest Science, Nanjing Forestry University, Nanjing 210037, China; zhangzh@njfu.edu.cn (Z.Z.); luoying.roy@foxmail.com (Y.L.); junstudent@126.com (X.W.)

[2] Yichun Forestry Industry Development Authority, Yichun 336000, China

* Correspondence: fyyu@njfu.edu.cn; Tel.: +86-025-8542-7403

Received: 24 March 2018; Accepted: 10 May 2018; Published: 12 May 2018


**Abstract:** Seed oil content is an important characteristic for the potential biofuel feedstock benzoin (*Styrax tonkinensis*). With the aim of further understanding benzoin lipid biosynthesis, the endosperm and embryo cell ultrastructures were acquired through transmission electron microscopy (TEM); the relative oil body area per cell (ROA) and oil body diameter (OBD) were then calculated by analyzing TEM images via computer software. The endosperm ROA peaked at 99 days after flowering (DAF) (79.04%), and the embryo ROA dynamic fitted the "S" curve. Significant linear relations ($p < 0.01$) were only observed between endosperm ROAs and the contents of whole-kernel crude lipid and fatty acids. The endosperm OBD (1.18–2.43 μm) was larger than that of embryo OBD (0.38–0.77 μm). M-shaped dynamics of acetyl coenzyme carboxylase (ACC) and diglyceride acyltransferase (DGAT) activities resembled the dynamic of endosperm OBD, as two peaks were observed at 78 and 113 DAF; the big oil body (≥1.8 μm) fraction in endosperm increased as kernel ACC and DGAT activities also increased, and vice-versa. Embryo OBD gradually increased, with the big oil body (≥0.5 μm) proportion increasing and the small oil body (<0.5 μm) proportion decreasing in general. Our results collectively suggested the distinct lipid accumulation patterns in the two benzoin kernel tissues, and revealed that the endosperm may determine the whole kernel oil biosynthetic process.

**Keywords:** *Styrax tonkinensis*; transmission electron microscopy; oil body; ultrastructure; endosperm; lipid accumulation

## 1. Introduction

Distributed in Vietnam, Laos, and the southern provinces of China, benzoin (*Styrax tonkinensis* (Pierre) Craib ex Hartwich) is now a renewable biofuel feedstock that may be used to address the worldwide food and energy crisis [1,2]. As such, benzoin oilseed has attracted the scientific interest of Chinese researchers [3].

Small spherical compartments called oil bodies, which are essentially compartments with triacylglycerol (TAG) cores, are assembled in plant cells [4,5]. For oilseed species, carbon storage and accumulation in these lipid droplets during seed maturation is an essential energy constituent for further seed germination and seedling growth [6–8]. The kernel lipid content of oilseed species varies greatly from 30 to 75% *w*/*w* [9], which is dependent on the TAG accumulation in oil bodies at the metabolic level [5,10]. In general, studies on developing seeds have indicated that acetyl-coenzyme A carboxylase (ACC) and diacylglycerol acyltransferase (DGAT) activities are associated with

lipid synthesis and these enzymes may catalyze a rate-limiting reaction in fatty acids and TAGs bioassembly [3,11,12].

Our previous paper [13] confirmed that the oil accumulation rate reduces during the mid-late stage of benzoin seed filling, as shown by in vitro physiological evidence in seeds. However, several contradictory results have been found in other oilseed species. In maize (*Zea mays*), reduction of the oil accumulation rate was only observed in one of five cultivated varieties [14]; a nearly 50% decrease in fatty acids concentration (on dry basis) was detected during the mid-late development stage in seeds of soybean (*Glycine max*) cultivar Zhongdou 8 [15], while the total lipid content in another soybean seed cultivar continued to increase before the oil synthesis stopped when the seeds matured [16]. Moreover, ACC activity was not considered to be closely correlated with the rate of lipid biosynthesis in maize [17] or rape (*Brassica napus*) [18]. In this study, we hope to obtain some direct biological evidence to further support the rare oil accumulation behavior in benzoin seeds.

In albuminous oilseeds, oil bodies can be found in the endosperm and embryo [10]. For high oil content genotypes of *Jatropha curcas* seeds, a higher expression of most of the fatty acid and TAG synthetic pathway genes was shown in endosperms compared to embryos, whereas, in low oil content genotypes, a significant difference was not found between endosperms and embryos [19]. This indicates the fundamental function of oilseed endosperms in determining the whole kernel lipid content.

In the present study, images of the *S. tonkinensis* endosperm and embryo cells were acquired using the transmission electron microscope technique, and the ultrastructure evolution of their oil bodies was then quantified by computer software. The aims of the study were to answer the following questions: (1) Would the in situ oil body morphology dynamic agree with our previous in vitro physiological data concerning benzoin oil accumulation speed loss? (2) If so, would any significant differences between endosperms versus embryos be found in oil accumulation patterns? (3) If so again, which part of the benzoin kernel has a better correlation with the lipid biosynthetic rhythm? Answers obtained through our investigation may help to clarify the understanding of the unique oil accumulation phenomenon in *S. tonkinensis*.

## 2. Materials and Methods

### 2.1. Plant Material

In 2012, *Styrax tonkinensis* seeds (from Jishui, Jiangxi, China) were purchased and sown on the southeast side of Hewang Lake, Luhe District, Nanjing, China (32°54′ N, 118°84′ E), where they grew under natural conditions. The benzoin plants' juvenile phase ended in 2014, and open pollination has been applied since then. In late May 2015, one sample tree was selected and tagged. The diameter at breast height (1.3 m above the ground) (DBH), total tree height, and number of flowers were measured in two consecutive years (Table 1). Fresh fruits were randomly harvested in different branch directions from the selected plant from 3 August (57 days after flowering (DAF)) to 19 October (134 DAF), with a seven-day interval between each harvest. Drupes were sealed in plastic bags and then embedded in a plastic foam box filled with ice packs (−10 °C) before the seeds were removed and sub-sampled.

**Table 1.** Diameter at breast height (DBH), total tree height, and number of flowers of the sampled *S. tonkinensis* tree in 2014 and 2015.

| Year | Tree Height (m) | DBH (cm) | Flowers per Tree |
|---|---|---|---|
| 2014 | 3.20 | 3.16 | 7656 |
| 2015 | 3.23 | 3.18 | 5990 |

### 2.2. Anatomical Observation

Fruits were vertically cut and photographed using a stereomicroscope (SZX16, OLYMPUS Co., Tokyo, Japan). Endosperm and embryo materials used for transmission electron microscopy (TEM)

(JEM-1400, JEOL, Tokyo, Japan) imaging were prepared via a method similar to that described previously [20]. Briefly, the samples were immediately fixed with 4% ($v/v$) glutaraldehyde in sodium phosphate buffer (pH 7.2), after which they were postfixed in osmium tetroxide, dehydrated, and embedded in Spurr's resin. Sections were observed at 60 kV with an electron microscope (JEM-1200, JEOL, Tokyo, Japan). The remaining seeds were immediately stored at −70 °C for lipid and enzyme analyses.

### 2.3. Lipid Analysis

Thirty de-coated seeds were weighed after drying at 60 °C for 48 h. The dry kernels were then ground and the seed oil was extracted with petroleum ether (30–60 °C) using a Soxhlet apparatus, as described by Gao [21]. The flask temperature was kept at 60 °C, and the extraction lasted 12 h. Lipid was then separated from the petroleum ether using a rotary vacuum evaporator at 60 °C. After extraction, the ground seeds were weighed again, and the total crude lipid (TCL) content was expressed as the percentage of oil on a dry weight basis. About 0.1 mL oil was first dissolved in 2 mL of petroleum ether/benzene (1:1, $v/v$) and then fully mixed with 2 mL of 0.4 mol/L KOH-$CH_3OH$ to prepare the fatty acid methyl esters (FAMEs). Following a previously reported method [13], the relative amount of each FAME component was quantified by gas chromatography-mass spectrometry (GC/MS) (ISQ, Thermo Fisher Scientific, Waltham, MA, USA). The total fatty acids (TFA) were then calculated using the combined FAMEs, and results were expressed as a percent of kernel dry weight. The triacylglycerol (TAG) measurements were conducted with kits (Suzhou Comin Biotechnology Co., Ltd., Suzhou, China) based on the acetylacetone colorimetric method of Sardesai and Manning [22].

### 2.4. Acetyl Coenzyme Carboxylase (ACC) and Diglyceride Acyltransferase (DGAT) Activities Analysis

Frozen de-coated seeds (500 mg) were used to analyze the presence of ACC and DGAT activities. ELISA (enzyme-linked immunosorbent assay) kits were provided by SHANGHAI RESUN TRADING Co., LTD. (Shanghai, China). The microtiter plates were pre-coated with an antibody specific to plant ACC (or DGAT). After antibody-antigen interactions, signals were amplified by the biotin-avidin system and the antigen targets in samples were qualified through an HRP (horseradish peroxidase)-TMB (3,3′,5,5′-tetramethylbenzidine) colorimetric detection system. The color change was measured spectrophotometrically at a wavelength of 450 nm. AAC (or DGAT) concentration in samples was then determined by comparing the optical density (OD) value to the standard curve.

### 2.5. Measurement of Oil Body Diameter and Relative Area

We analyzed all of the oil bodies seen in the endosperm or embryo TEM images at each seed development stage. In the mid-late seed development stage, a new type of embryo cell was differentiated, which was located mostly in the young axis and radicle. TEM images are shown in Figure S1. Organelles such as the nucleus and endoplasmic reticulum, rather than oil bodies, filled these cells. In this study, this type of cell was not included during the analysis.

For embryo tissue preparation for detailed analysis, we always selected and compared the same two sections along the cotyledon mid-axis; for endosperm, tissue from near the cotyledon was used for TEM analysis (Figure S2). The TEM image was viewed in Nano Measurer 1.2 (Fudan University, Shanghai, China, 2008). Since the shape of most oil bodies was oval shaped, for each individual oil body, the short ($\alpha$) and long elliptical axis ($\beta$) were measured (Figure 1a). The standard rulers in the images were set as references for measurement (same hereafter). The oil body diameter (*OBD*) was calculated as:

$$OBD = \frac{\alpha + \beta}{2} \quad (1)$$

The relative oil body areas were determined using AutoCAD 2010 (Autodesk Inc., Manchester, NH, USA). The outline of each cell (red circle in Figure 1b) and the oil bodies within the cell (blue dashed circles in Figure 1b) were drawn by using the *Polyline* (PL) command. The corresponding

cell area ($A_{cell}$) and the collective oil body area ($A_{COA}$) were obtained by usingr the *Area* (A) command. The relative oil body area (*ROA*) was determined by the following equation:

$$ROA = \frac{A_{COA}}{A_{cell}} \times 100\% \quad (2)$$

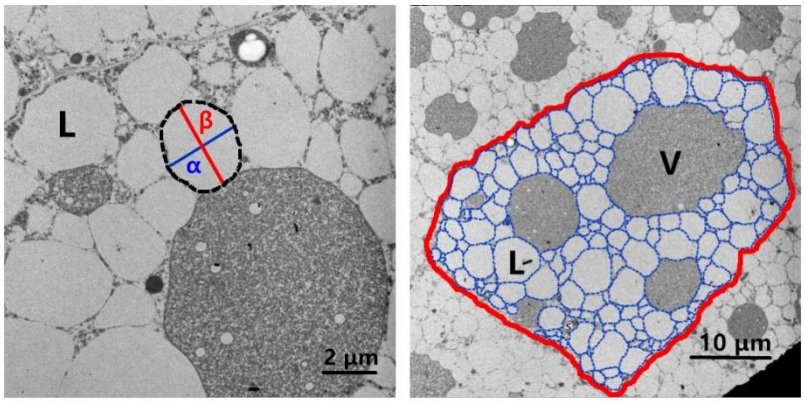


(**a**) (**b**)

**Figure 1.** Rules to quantify the oil body ultrastructure in benzoin endosperm and embryo cells. (**a**) For each individual oil body (black dashed circle) diameter, the elliptical short ($\alpha$) and long axis ($\beta$) were measured; (**b**) The outline of an individual cell (red circle) and the oil bodies within it (blue dashed circles). L, lipid body; V, vacuole.

### *2.6. Statistics Analysis*

Values were expressed as means ± SD of three independent experiments. Excel (Office 2013 Pro Plus, Microsoft Corporation, Redmond, WA, USA) was used to process figures. One-way analysis of variance (ANOVA) was performed using SPSS 19.0 (IBM, Armonk, NY, USA), and followed by Duncan's Multiple Range Test. *p*-values less than 0.05 were considered significant within groups. A regression analysis was conducted between oil body relative area and kernel lipid content, while associations between oil body diameter variables and lipid synthesis-related enzyme activities were determined using Pearson's correlation analysis.

## 3. Results

### *3.1. Change of Seed Morphology and Cell Ultrastructure*

A boundary between the milky-white endosperm and the benzoin seed coat could be clearly identified at 57 DAF (Figure 2a). The kernel remained unenlarged at 85 DAF; however, the axis and cotyledon (i.e., embryo) were already differentiated at this timepoint. The endosperm and embryo grew substantially and filled almost the whole benzoin seed over the next 35 days, which was accompanied by darkening and hardening of the seed episperm. The cell ultrastructure varied between the endosperm and embryo as the cell evolved (Figure 2b). Lipid bodies gradually filled the endosperm cells; changes in the area of the irregular cell correlated well with kernel morphology. Furthermore, cell walls thickened continuously over time. Unlike the endosperm, a relatively similar area proportion of the circular cell was found in *S. tonkinensis* embryos at 85 and 120 DAF. Furthermore, a few starch granules could be identified at the two time points.

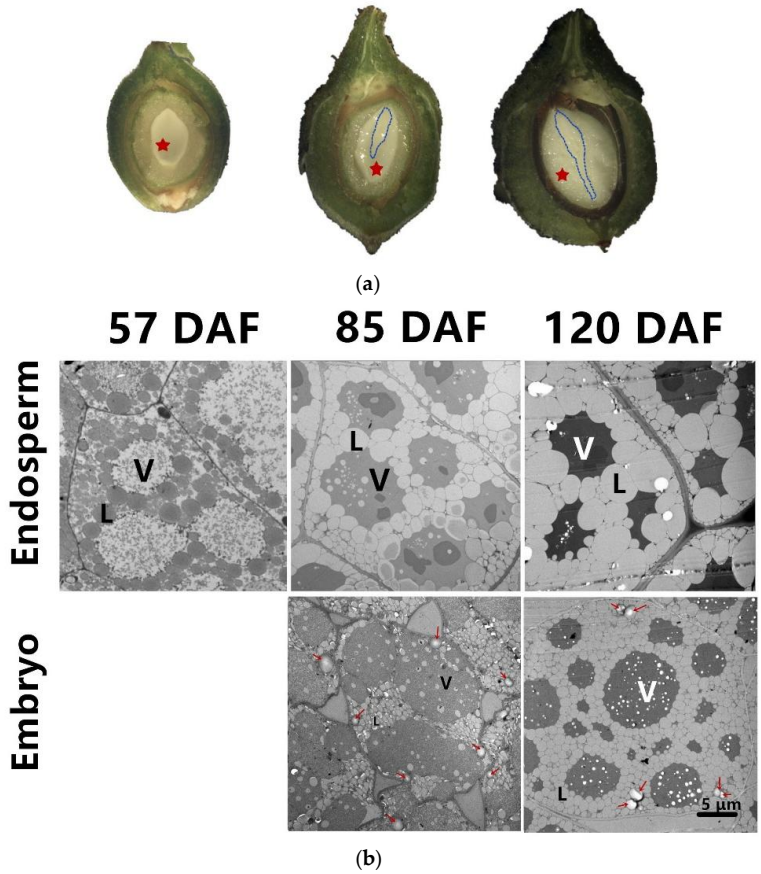


**Figure 2.** Change of seed morphology and cell ultrastructure. (**a**) Photographs show longitudinal sections of fruits at 57, 85, and 120 days after flowering (DAF). Blue dashed dots outline the embryo, and red pentagrams indicate the endosperm; (**b**) Ultrastructure of endosperm and embryo at 57, 85, and 120 DAF visualized by transmission electron microscopy (TEM). Starch granules were indicated by red arrows. L, lipid body; V, vacuole.

### *3.2. ROA Evolution in Endosperm and Embryo Cells*

To demonstrate the difference between the benzoin endosperm and embryo cells in terms of oil accumulation, we analyzed the ROA and the relationship of decoated seed lipid content with endosperm and embryo ROA. In endosperm cells (Figure 3a), the ROA peaked at 99 DAF (79.04%); thereafter, the ROA decreased gradually over the next 21 days. For the *S. tonkinensis* embryo (Figure 3b), the oil body proportion per cell remained relatively unchanged from 64 to 78 DAF, ranging from 25.95 to 35.26%. A large 76% increase was observed between 78 and 99 DAF. The embryo ROA then rose to a plateau at 62.00% (99 DAF) to 66.41% (120 DAF).

Significant linear relations were observed between the ROA in endosperm cells and all three kernel lipid variables (Figure 4). However, for embryo cells, ROA was only significantly linearly correlated with the TAG; moreover, our data in Figure 4 shows that a more closed relationship was found between ROA and TFA (rather than TCL), and the highest correlation of ROA was observed with TAG.

Lipid dynamics are provided in Figure S3. In general, the TCL, TFA, and TAG dynamics all exhibited up-and-down patterns. For both TCL and TFA, peak concentrations were found at 85 DAF, and decreasing trends were then observed between 85 and 120 DAF, with a 19.74% and a 19.81% decrease for TCL and TFA, respectively. Similarly, the TAG concentration of the developing *S. tonkinensis* kernel increased gradually until 99 DAF (14 days after the TCL and TFA peaks), and then, a decreasing trend was detected for the next 21 days.

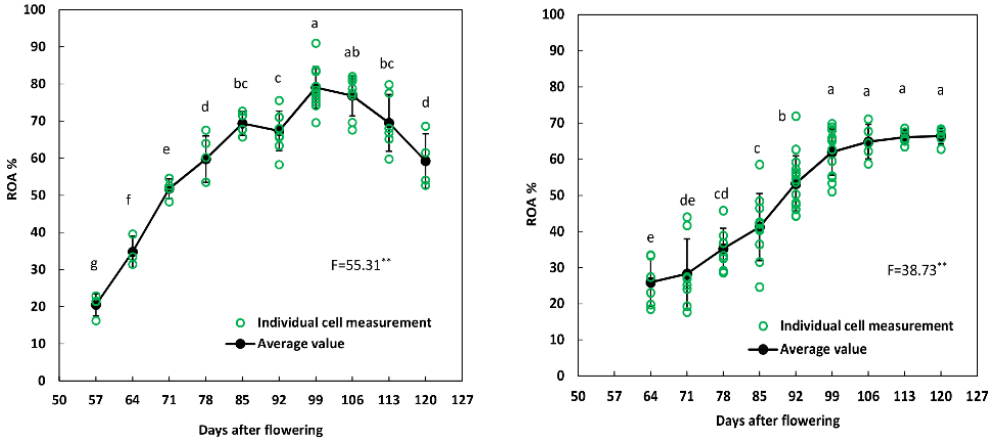


**Figure 3.** Relative oil body area (ROA) dynamics in benzoin endosperm (**a**) and embryo (**b**) cells. ** indicates significance at $p < 0.01$. Different letters within days after flowering (DAF) indicate significant ROA difference for endosperm or embryo cells ($p < 0.05$).

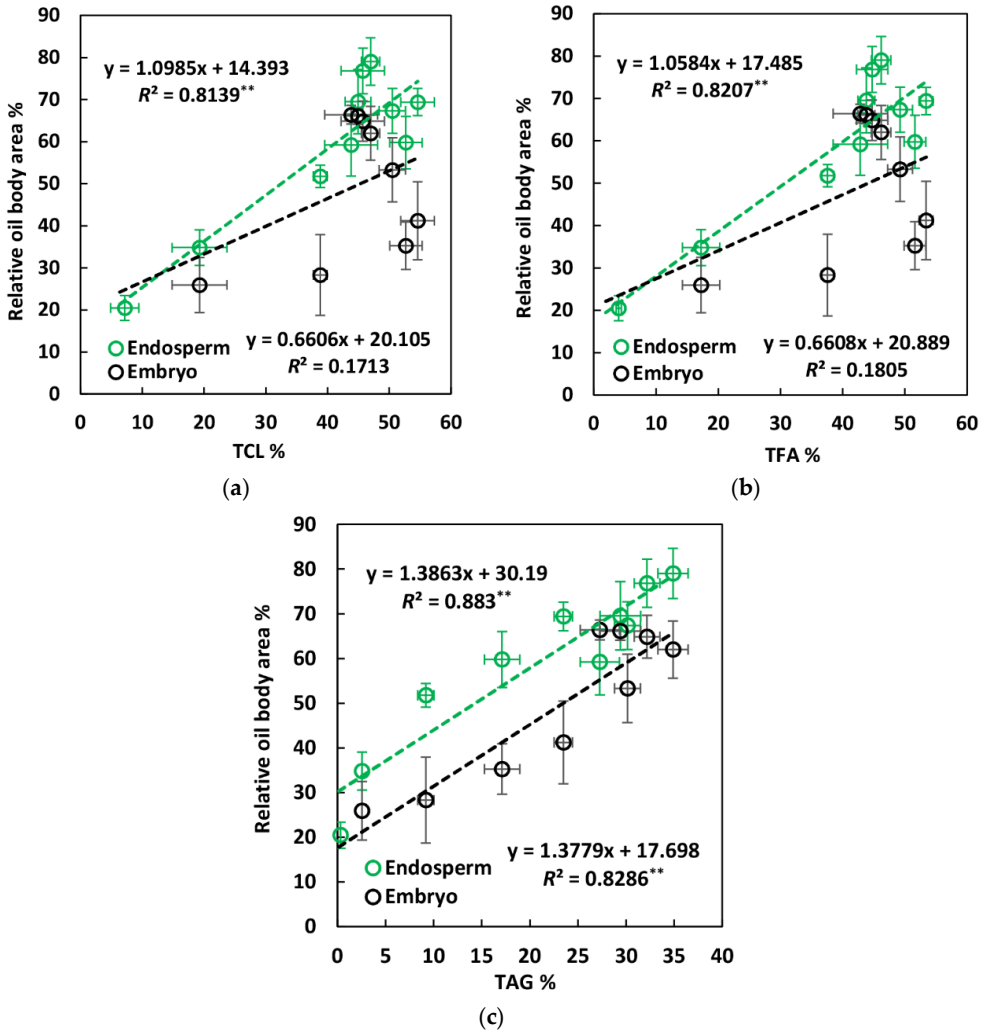


**Figure 4.** Regression analysis between ROA of the two different kernel tissues and total crude lipid concentration (**a**), total fatty acid concentration (**b**), and total triacylglycerol concentration (**c**), respectively. ** indicates linear regression significance at $p < 0.01$.

### *3.3. Changes in Key Enzyme Activities during Seed Lipid Synthesis*

Dynamics of ACC activity followed an M-shaped trend. Peaks were found along with the lipid accumulation process, at 78 and 120 DAF (Figure 5a). DGAT activity had a single peak at 78 DAF (Figure 5b). It then dropped continuously until 21 days later (99 DAF), yet, unlike the ACC activity, it continued to rise after 120 DAF and reached 1.7 U/L at 134 DAF.

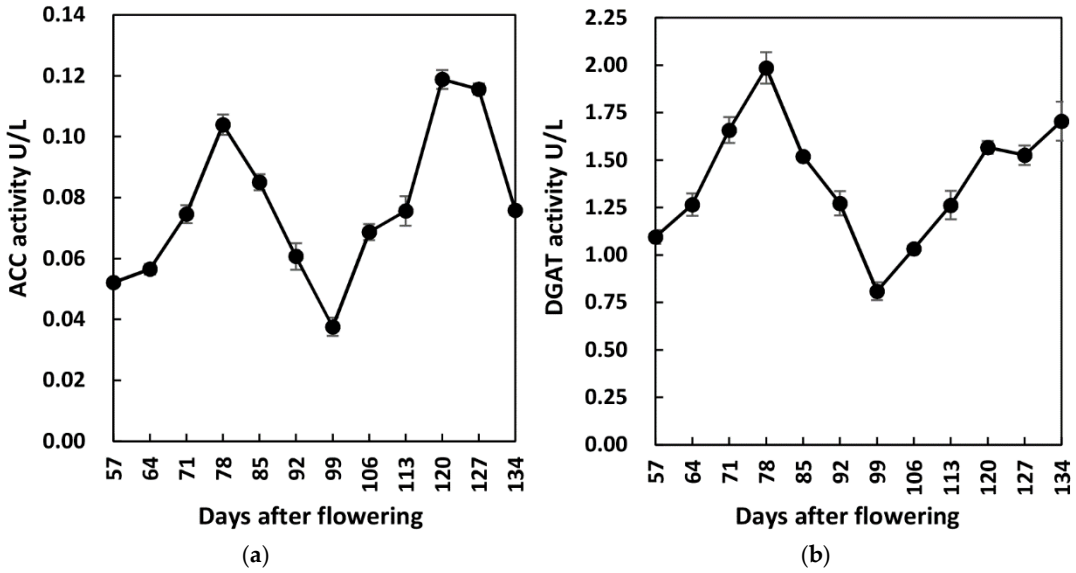


**Figure 5.** Dynamics of oil biosynthesis-related enzyme activities in benzoin kernel. (**a**) Acetyl coenzyme carboxylase (ACC) activity dynamic; (**b**) Diglyceride acyltransferase (DGAT) activity dynamic.

### *3.4. Changes of OBD in Endosperm and Embryo Cells*

Profound OBD changes during *S. tonkinensis* seed development are demonstrated in Figure 6. Endosperm OBD saw its first peak at 78 DAF (Figure 6a). It then dropped over the next 14 days; thereafter, it rose linearly and peaked again at 113 DAF, with a 70.1% increase. The diameter distribution of endosperm oil body was investigated and shown in Figure 7. Average oil body in the embryo shrank from 64 to 78 DAF (Figure 6b); OBD then increased slowly before a remarkable 48.1% rise from 99 to 106 DAF, after which it reached a plateau (0.71–0.77 μm). The embryo OB numbers of different sizes are further illustrated in Figure 8.

We then analyzed the proportion of different oil body sizes at all kernel development stages. Specifically, 0.2–0.6 and 0.6–1.0 μm oil bodies in endosperm cells showed a W-shape pattern (Figure S4); the lowest values were found at 78 and 113 DAF. The proportion level of 1.8–4.2 μm oil bodies increased continuously and initially peaked at 71 or 78 DAF. Thereafter, the second peak was seen at 106 or 113 DAF. Other oil bodies with a size of more than 4.2 μm appeared after 71 DAF, and they only represented less than 5% of oil body numbers, cumulatively.

Figure S5 shows the embryo oil body composition in different sizes. Fractions of 0.2–0.3, 0.3–0.4, and 0.4–0.5 μm oil bodies rose from 64 to 78 DAF. They then descended dramatically until 120 DAF, with a 100%, 92.9%, and 91.1% decline, respectively. Oil bodies with a size of 0.8–1.1 μm remained unseen until 85 DAF, and they all evolved progressively in the next 35 days. Larger oil bodies (≥1.1 μm) were found after 99 DAF; a transient accumulation was observed from 99 to 106 DAF.

In general, the big oil body (BOB) (≥1.8 μm) fraction in endosperm cells increased from 57 to 78 DAF (Figure 9a). It then showed a fall-and-rise tendency and reached its second peak at 113 DAF. The endosperm small oil body (SOB) (0–1.8 μm) composition dynamics showed a pattern opposite that of BOB. The young embryo cells contained approximately equal amounts of SOB (0–0.5 μm) and BOB (≥0.5 μm) at 50 DAF (Figure 9b). The oil body composition changed rapidly afterwards.

Overall, the SOB fraction peaked at 78 DAF and dropped in the next 42 days, with a large 83.2% decrease. Meanwhile, the BOB proportion generally had a 1.8-fold increase through the embryo cell development stages.

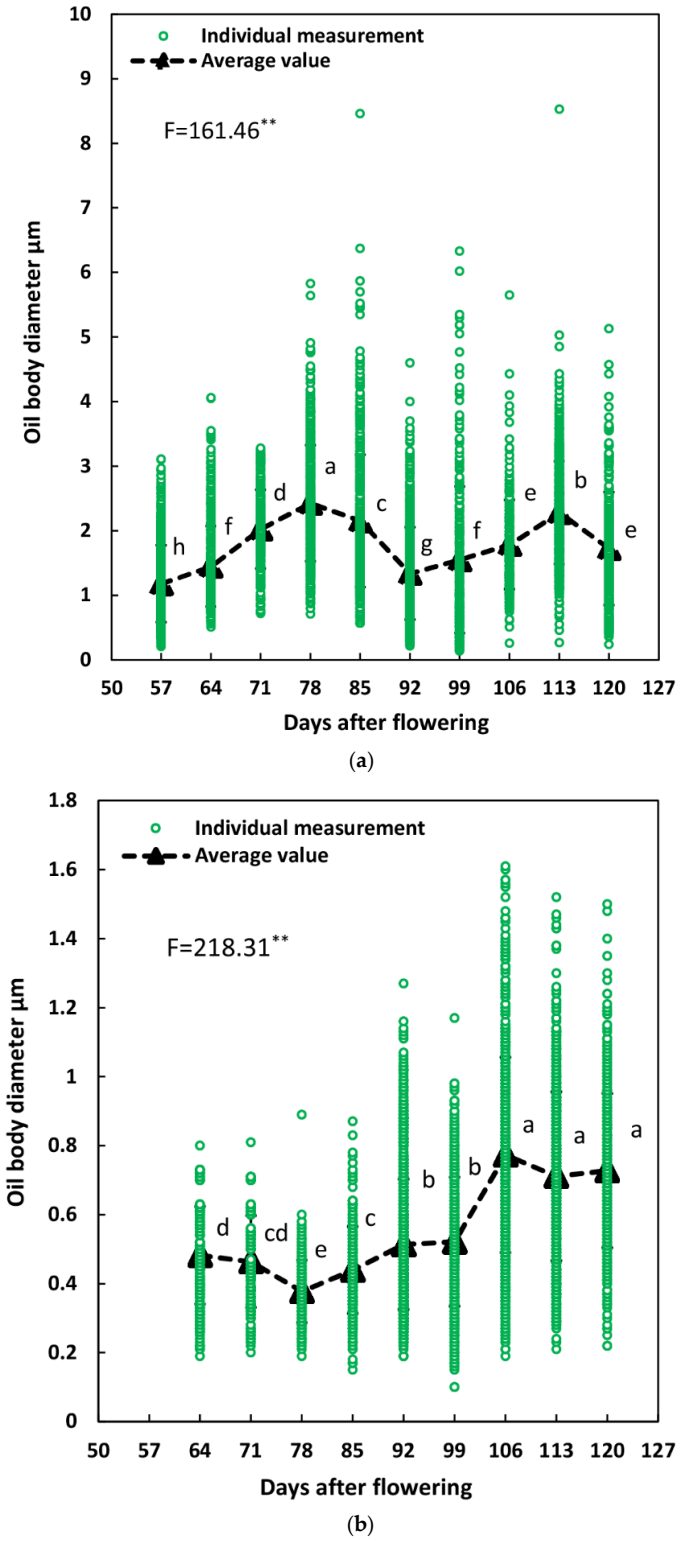


**Figure 6.** Dynamics of oil body diameter (OBD) in benzoin endosperm (**a**) and embryo (**b**) cells. ** indicates significance at $p < 0.01$. Different letters within days after flowering (DAF) indicate significant OBD difference for endosperm or embryo cells ($p < 0.05$).

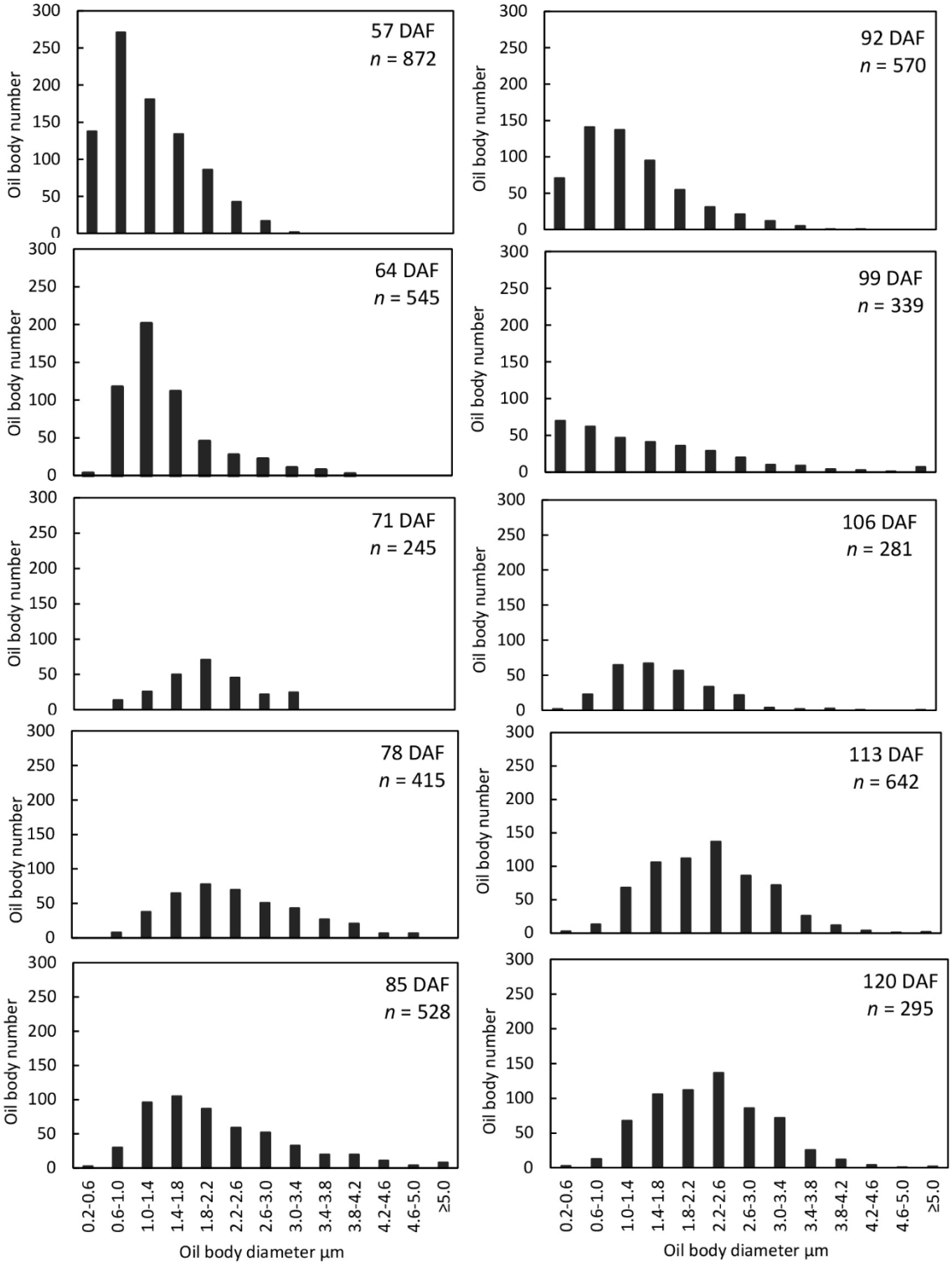


**Figure 7.** The oil body numbers of various sizes at different development stages in benzoin endosperm cells. The total OB number investigated at each development stage is indicated with "*n*".

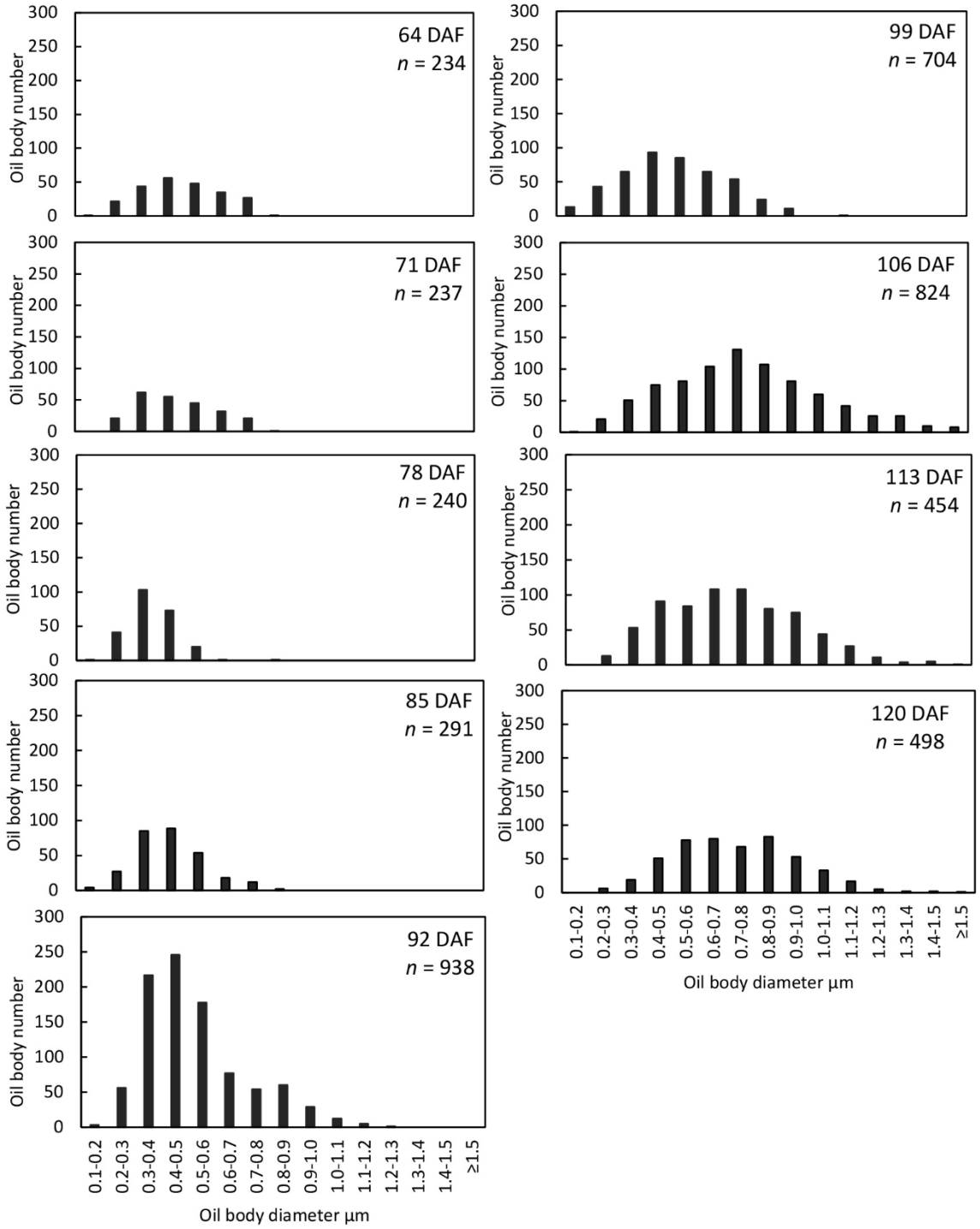


**Figure 8.** The oil body numbers of various sizes at different development stages in benzoin embryo cells. The total OB number investigated at each development stage is indicated with "*n*".

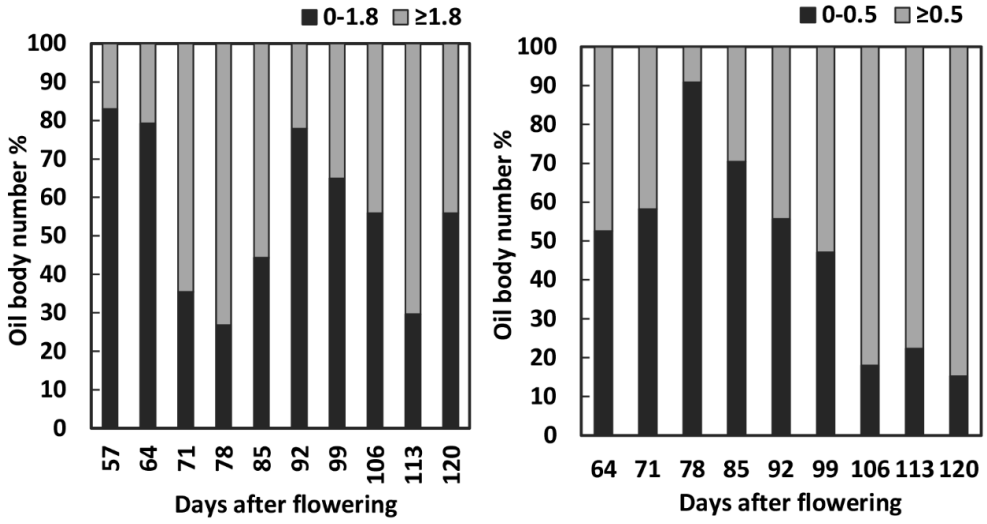


**Figure 9.** Oil body fractions in benzoin kernel cells. (**a**) Big oil body (≥1.8 μm) and small oil body (0–1.8 μm) composition in endosperm; (**b**) Big oil body (≥0.5 μm) and small oil body (0–0.5 μm) composition in embryo.

## 4. Discussion

### *4.1. Endosperm and Embryo Cells Exhibit Differential Oil Deposition Patterns*

The endosperm and embryo development of angiosperm seeds initiates from double fertilization [23,24], through which the two dissimilar tissues acquire different ploidies, i.e., genetic background; therefore, morphological and functional regulations are displayed in distinct ways, which may greatly impact metabolic pathways such as lipid biosynthesis during seed formation [25].

In this study, ROA was introduced to evaluate the oil deposition process. Our quantitative ultrastructural determination results indicated that the endosperm and embryo cells exhibited two different ways to accumulate lipids in benzoin (Figure 3). However, the decrease in oil accumulation rate was only observed in endosperms, with a nearly 25% decrease in ROA observed between 99 and 120 DAF (Figure 3a). Therefore, we ask how we could assess the ROA in endosperm and embryo cells as a whole. Unlike argan seed, in which two main tissues (embryo and endosperm) contribute equally to kernel volume [25], the embryo only occupies up to 10% of the volume in benzoin kernel (data not shown). We thus made a rough estimate of the whole-kernel oil body volume (Figure 10) based on the volume ratio between the endosperm and embryo. The kernel ROA dynamic turned out to be closely correlated to endosperm cells, which again suggested a reduced oil accumulation rate during benzoin seed development. Notably, cotyledon cells, which are the main storage tissues and the main location of TAG accumulation on the whole-embryo level [19], were selected to calculate the embryo ROA in the present study; the actual embryo ROA value, therefore, could be lower than the determined value.

The benzoin embryo and endosperm accumulated an equal amount of oil bodies at 120 DAF (Figure 3a,b), but the dry weight and tissue volume of the endosperm was higher (data not shown). On the contrary, the lipid content of the embryo is relatively low as compared to that of the endosperm and seed coat in the *Jatropha curcas* mature seed [19,26,27]. Although ROA would not necessarily represent the cell lipid content level, our collective evidence indicated the different oil deposition patterns within the two main tissues. In general, the benzoin endosperm deposited large amounts of lipid during the early-mid stages of kernel development (which was supported by ROA data), while the embryo accumulated oil continuously throughout its development, yet at a moderate rate. It is noteworthy that the DGAT measurement (Figure 5) in the whole kernel suggests an active oil deposition between 99 and 120 DAF, though endosperm ROA dropped during this 21 days. So is it

really a slow-down of oil deposition? We'd like to state that TAG content (%) in the whole kernel dropped between 99 and 120 DAF (Figure S3), which correlates with the decrease of endosperm ROA. So, the question is, why did endosperm ROA have a 25% decrease when DGAT indicates an active oil deposition? We believe it is the enzyme unit (U/L) that causes this confusion. When we take the protein content (mg/g FW) in the DGAT extract into consideration (which will make the enzyme unit into U/mg protein), the relative DGAT (U/mg protein) actually slows between 99 and 113 DAF (data not shown).

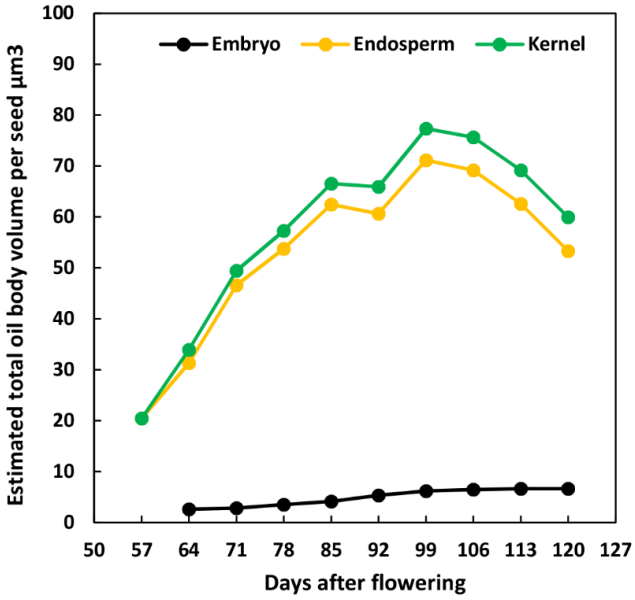


**Figure 10.** The estimated total oil body volume per seed (ETOV) in benzoin embryo, endosperm, and kernel. We assumed that the endosperm and embryo had 90 and 10 cells, respectively (each cell's volume is 1 $\mu m^3$), plus the ROA was used to represent the relative oil body volume. So, $ETOV_{kernel}$ = $ETOV_{endosperm}$ + $ETOV_{embryo}$ = 90 × $ROA_{endosperm}$ + 10 × $ROA_{embryo}$.

### *4.2. Benzoin Endosperm Determines Kernel Lipid Content*

The distinct destinies of endosperm and embryo originate from the double fertilization event. In addition to providing mechanical support during young embryo growth and maintaining a high osmotic potential around the embryo [28,29], the fundamental function of the hypertrophic endosperm is to provide the embryo with nutrient sources such as carbon, nitrogen, and minerals [26,29,30]. High metabolic activity associated with starch accumulation is specifically assigned to the endosperm in grain seeds such as maize [24] and wheat (*Triticum aestivum*) [31], while the transcript abundance of some lipid-biosynthesis-related genes are 10-fold-higher in the endosperm than in the embryo of the oilseed *Jatropha curcas* [19]. The *S. tonkinensis* endosperm is highly comparable to the embryo in both volume and dry weight; our regression analysis, shown in Figure 4, clearly demonstrated a significant correlation between the kernel lipid content (TCL and TFA) and the endosperm ROA (rather than that of the embryo). Such phenomena have also been observed in castor (*Ricinus communis*) [32] and argon (*Argania spinosa*) [25] seeds.

The benzoin endosperm and embryo ROA were most closely related with the TAG (among the three lipid content indices). This result could be easily explained by the fact that oil bodies are accumulated by cells to store TAGs. TFA represents most of the crude oil in the development of benzoin decoated seeds [13]. As shown in Figure S3, lipophilic substances accounted for 44.2% of the total crude fat at 57 DAF. This proportion dropped thereafter when the TFA content increased to more than 90% of the total crude oil. As the lipophilic substances are not stored in the oil body, it is reasonable that the lowest $R^2$ was observed between TCL and ROA.

### *4.3. Relationship between Rate-Limiting Enzyme Activity and Oil Body Size Reveals Oil Biosynthesis Rhythm*

Much research has focused on finding the regulatory points of plant fatty acids synthesis. Evidence retrieved in a wide variety of species (both through in vivo and in vitro experiments) points to ACC activity as the determinant control over lipid biosynthesis [33]. In addition, transgenic technology has been used in several dicot plants, such as canola [34] and soybean [35], after *DGAT1* was suggested to play a key role in seed lipid formation; increased DGAT activity and seed oil content were observed in these experiments [36]. The ACC and DGAT activities were hence determined during benzoin kernel development. The Pearson's correlation was then further analysed between the activities of two major oil biosynthetic pathway regulatory enzymes and the endosperm OBD. The results indicated the positive impact of the two oil synthesis rate-limiting enzymes on the endosperm oil body sizes (ACC: $R = 0.844$, $p < 0.01$; DGAT: $R = 0.676$, $0.01 < p < 0.05$). Therefore, to provide insight on discriminating endosperm and embryo with respect to the control of crucial lipid synthesis enzymes in the development of *S. tonkinensis* kernel OBD, we further calculated the Pearson's correlation index between enzyme activities and the oil body proportions under various OBD ranges (Table 2). In benzoin endosperm cells, negative correlations were found between the small oil bodies' proportion (with an OBD less than 1.8 μm) and the rate-limiting enzyme. Furthermore, when ACC and DGAT activities increased, the number of relatively big oil bodies (≥1.8 μm) also increased, and vice-versa. Specifically, ACC and DGAT activity cleavage from 78 to 120 DAF (Figure 5) greatly correlated with the endosperm oil body OBD during the corresponding 42 days. However, almost no significant linear relation could be found between the oil body size and the activities of the two key enzymes investigated.

**Table 2.** Correlation analysis between enzymatic and oil body ultrastructure variables in all development stages of benzoin de-coated seeds. (Pearson's coefficients, two-tailed).

| Variables | | Kernel Enzyme Activity (U/L) | |
|---|---|---|---|
| | | ACC | DGAT |
| Endosperm oil body number (%) with the corresponding OBD (μm) | 0.2–0.6 | −0.762 * | −0.643 |
| | 0.6–1.0 | −0.763 * | −0.559 |
| | 1.0–1.4 | −0.431 | −0.372 |
| | 1.4–1.8 | 0.287 | 0.136 |
| | 0–1.8 | −0.783 * | −0.675 * |
| | 1.8–2.2 | 0.733 * | 0.47 |
| | 2.2–2.6 | 0.635 | 0.342 |
| | 2.6–3.0 | 0.762 * | 0.569 |
| | 3.0–3.4 | 0.642 | 0.438 |
| | 3.4–3.8 | 0.642 | 0.502 |
| | 3.8–4.2 | 0.769 * | 0.6 |
| | 4.2–4.6 | 0.591 | 0.426 |
| | 4.6–5.0 | 0.729 * | 0.688 * |
| | ≥5.0 | −0.295 | −0.403 |
| | ≥1.8 | 0.783 * | 0.675 * |
| Embryo oil body number (%) with the corresponding OBD (μm) | 0.1–0.2 | −0.504 | −0.457 |
| | 0.2–0.3 | 0.385 | 0.632 |
| | 0.3–0.4 | 0.631 | 0.849 ** |
| | 0.4–0.5 | 0.345 | 0.625 |
| | 0–0.5 | 0.008 | 0.540 |
| | 0.5–0.6 | −0.592 | −0.264 |
| | 0.6–0.7 | −0.724 * | −0.704 |
| | 0.7–0.8 | −0.583 | −0.759 * |
| | 0.8–0.9 | −0.245 | −0.604 |
| | 0.9–1.0 | −0.111 | −0.488 |
| | 1.0–1.1 | 0.02 | −0.376 |
| | 1.1–1.2 | −0.002 | −0.404 |
| | 1.2–1.3 | 0.013 | −0.385 |
| | 1.3–1.4 | −0.014 | −0.372 |
| | 1.4–1.5 | 0.027 | −0.376 |
| | ≥1.5 | −0.018 | −0.369 |
| | ≥0.5 | −0.008 | −0.540 |

Note: * indicates significant correlation at $0.01 < p < 0.05$, and ** indicates significant correlation at $p < 0.01$ by Pearson's correlation coefficients analysis.

These observed correlations have two implications for understanding the oil accumulation process of *S. tonkinensis*. First, the benzoin endosperm and embryo do not contribute equally to the lipid

yield during seed formation as the endosperm cells are largely associated with the kernel oil synthesis event. Second, oil biosynthetic pathway enzymes may control the sizes of oil bodies. Notably, the synchronized evolutionary pattern was not observed for endosperm ROA and OBD dynamics. According to the ACC and DGAT activities dynamics (Figure 5) and the total fatty acids concentration (Figure S3), the rate of kernel oil synthesis in benzoin decreased at 78 DAF, resulting in an increase in the proportion of small oil bodies; the average OBD, therefore, declined from 78 to 92 DAF (Figure 6), whereas the total oil body area continued to increase, although at a much slower rate than that seen earlier (Figure 3).

## 5. Conclusions

In this study, to the best of our knowledge, we reported the first TEM images of developing *S. tonkinensis* kernel cells. The unique decrease in the oil accumulation rate was again verified by our very direct and accurate quantitative ultrastructural data. Distinct lipid accumulation patterns were observed in the two benzoin kernel tissues, and the endosperm may determine the whole-kernel oil biosynthetic process, as the endosperm (rather than embryo) ROA and OBD were found to be highly correlated with the kernel lipid content and activities of rate-limiting enzymes involved in oil synthesis during seed filling.

## 6. Limitation and Outlook

The dynamics of oil contents, starch contents, and enzyme activities in the benzoin endosperm and embryo should be measured separately to consolidate our standpoint.

From a research perspective, in order to distinguish the molecular mechanism differences in lipid synthesis presented in the benzoin endosperm and embryo, we intend to conduct a comparative proteome and transcriptome analysis of the developing endosperm and embryo in the near future. This could provide us with a deeper understanding of how to increase the oil yield in the potential biofuel feedstock benzoin.

**Supplementary Materials:** The following are available online at http://www.mdpi.com/1999-4907/9/5/265/s1, Figure S1: Two types of TEM images in *Styrax tonkinensis* embryo cells during seed development. Type A was found in cotyledons, and Type B was mostly found in axis. L, lipid body; Nu, nucleolus; V, vacuole; ER, Endoplasmic reticulum. Figure S2: The kernel sections selected for TEM study are shown. Two sections (indicated by the yellow dashed dots) along the cotyledon mid-axis (red dashed line) are chosen for the embryo TEM qualification analysis. Two endosperm sections near the cotyledon (indicated by the black dots) are used for endosperm ROA and OBD. Figure S3: Total crude lipid (TCL), total fatty acids (TFA) and triacylglycerol (TAG) concentration (100% $\times$ $w/w$) in the developing dry kernels of *Styrax tonkinensis*. Figure S4: Dynamics of oil body number proportions under various OB sizes (μm) in benzoin endosperm cells. OB sizes were indicated in each line chart. Figure S5: Dynamics of oil body number proportions under various OB sizes (μm) in benzoin embryo cells. OB sizes were indicated in each line chart.

**Author Contributions:** F.Y. and Y.L. conceived and designed the experiments; Y.L. and X.W. performed the experiments; Z.Z. and Y.L. analyzed the data; X.W. contributed reagents/materials/analysis tools; Z.Z. wrote the paper.

**Acknowledgments:** The authors acknowledge the funding received from a project funded by the Priority Academic Program Development of Jiangsu Higher Education Institutions (PAPD) and the Three New Agricultural Project of Jiangsu Province: Demonstration and Promotion of Effective Nurturing Techniques for *Styrax tonkinensis* as Seedlings and Grown Trees (ZX2014S0020).

**Conflicts of Interest:** The authors declare that they have no conflict of interest.

## References

1. Shi, G.; Zhu, G.; Huang, H.; Li, Y.; Liu, X.; Ye, X. Refining and toxicology preliminary evaluation of *Styrax tonkinesis* seed oil. *J. Chin. Inst. Food Sci. Technol.* **2014**, *14*, 192–201. (In Chinese)
2. Chen, W.; Li, L.; Liu, G.; Dong, Z.; Huang, Z.; Liu, H.; Chen, X.; Yu, W. Response surface methodology to optimize production of biodiesel from *Styrax tonkinensis*. *Guangzhou Chem. Ind.* **2015**, *43*, 46–49. (In Chinese)

3. Zhang, Z.; Luo, Y.; Wang, X.; Yu, F. Fruit spray of 24-Epibrassinolide and fruit shade alter pericarp photosynthesis activity and seed lipid accumulation in *Styrax tonkinensis*. *J. Plant Growth Regul.* **2017**, 1–19. [CrossRef]
4. Murphy, D.J.; Vance, J. Mechanisms of lipid-body formation. *Trends Biochem. Sci.* **1999**, *24*, 109–115. [CrossRef]
5. Liu, H.; Wang, C.; Chen, F.; Shen, S. Proteomic analysis of oil bodies in mature *Jatropha curcas* seeds with different lipid content. *J. Proteom.* **2015**, *113*, 403–414. [CrossRef] [PubMed]
6. Tzen, J.T.; Cao, Y.Z.; Laurent, P.; Ratnayake, C.; Huang, A.H. Lipids, proteins, and structure of seed oil bodies from diverse species. *Plant Physiol.* **1993**, *101*, 267–276. [CrossRef] [PubMed]
7. Ohlrogge, J.; Browse, J. Lipid biosynthesis. *Plant Cell* **1995**, *7*, 957–970. [CrossRef] [PubMed]
8. Beisson, F.; Fert, N.; Bruley, S.; Voultoury, R.; Verger, R.; Arondel, V. Oil-bodies as substrates for lipolytic enzymes. *Biochim. Biophys. Acta* **2001**, *1531*, 47–58. [CrossRef]
9. Anil, V.S.; Harmon, A.C.; Rao, K.S. Temporal association of $Ca^{2+}$-dependent protein kinase with oil bodies during seed development in *Santalum album* L.: Its biochemical characterization and significance. *Plant Cell Physiol.* **2003**, *44*, 367–376. [CrossRef] [PubMed]
10. Siloto, R.M.; Findlay, K.; Lopez-Villalobos, A.; Yeung, E.C.; Nykiforuk, C.L.; Moloney, M.M. The accumulation of oleosins determines the size of seed oilbodies in Arabidopsis. *Plant Cell* **2006**, *18*, 1961–1974. [CrossRef] [PubMed]
11. Jako, C.; Kumar, A.; Wei, Y.; Zou, J.; Barton, D.L.; Giblin, E.M.; Covello, P.S.; Taylor, D.C. Seed-specific over-expression of an Arabidopsis cDNA encoding a diacylglycerol acyltransferase enhances seed oil content and seed weight. *Plant Physiol.* **2001**, *126*, 861–874. [CrossRef] [PubMed]
12. Klaus, D.; Ohlrogge, J.B.; Neuhaus, H.E.; Dörmann, P. Increased fatty acid production in potato by engineering of acetyl-CoA carboxylase. *Planta* **2004**, *219*, 389–396. [CrossRef] [PubMed]
13. Zhang, Z.; Wang, X.; Luo, Y.; Yu, F. Carbon competition between fatty acids and starch during benzoin seeds maturation slows oil accumulation speed. *Trees–Struct. Funct.* **2017**, *31*, 1025–1039. [CrossRef]
14. Gan, F.; Zhang, Y.; Wu, Z. Research of oil accumulation in micro-endosperm super-high oil corn and Gaoyou115 corn. *J. Maize Sci.* **2009**, *17*, 18–21. (In Chinese)
15. Li, X.; Wu, G.; Wu, Y.; Xiao, L.; Lu, C. The accumulation pattern of fatty acids during the development of soybean seeds. *Soybean Sci.* **2007**, *26*, 506–510. (In Chinese) [CrossRef]
16. Qiu, L.; Wang, J.; Meng, Q. A preliminary study on the characteristics of protein and fat accumulation in soybean seeds. *Sci. Agric. Sin.* **1990**, *23*, 28–32. (In Chinese)
17. Gan, F.; Wu, Z. Research on the changes of acetyl-CoA carboxylase activity in the micro-endosperm maize during kernel development. *J. Maize Sci.* **2010**, *18*, 82–85. (In Chinese)
18. Kang, F.; Christopher, J.; Ridout, C.L.; Morgan, S.R. The activity of acetyl-CoA carboxylase is not correlated with the rate of lipid synthesis during development of oilseed rape (*Brassica napus* L.) embryos. *Planta* **1994**, *193*, 320–325. [CrossRef]
19. Sood, A.; Chauhan, R.S. Regulation of FA and TAG biosynthesis pathway genes in endosperms and embryos of high and low oil content genotypes of *Jatropha curcas* L. *Plant Physiol. Biochem.* **2015**, *94*, 253–267. [CrossRef] [PubMed]
20. Chen, M.; Wang, Z.; Zhu, Y.; Li, Z.; Hussain, N.; Xuan, L.; Guo, W.; Zhang, G.; Jiang, L. The effect of *TRANSPARENT TESTAR2* on seed fatty acid biosynthesis and tolerance to environmental stresses during young seedling establishment in Arabidopsis. *Plant Physiol.* **2012**, *160*, 1023–1036. [CrossRef] [PubMed]
21. Gao, J. *Experimental Guidance for Plant Physiology*; High Education Press: Beijing, China, 2006. (In Chinese)
22. Sardesai, V.M.; Manning, J.A. The determination of triglycerides in plasma and tissues. *Clin. Chem.* **1968**, *14*, 156–161.
23. Chaudhury, A.M.; Koltunow, A.; Payne, T.; Luo, M.; Tucker, M.R.; Dennis, E.S.; Peacock, W.J. Control of early seed development. *Annu. Rev. Cell Dev. Biol.* **2001**, *17*, 677–699. [CrossRef] [PubMed]
24. Lu, X.; Chen, D.; Shu, D.; Zhang, Z.; Wang, W.; Klukas, C.; Chen, L.; Fan, Y.; Chen, M.; Zhang, C. The differential transcription network between embryo and endosperm in the early developing maize seed. *Plant Physiol.* **2013**, *162*, 440–455. [CrossRef] [PubMed]
25. Errouane, K.; Doulbeau, S.; Vaissayre, V.; Leblanc, O.; Collin, M.; Kaid-Harche, M.; Dussert, S. The embryo and the endosperm contribute equally to argan seed oil yield but confer distinct lipid features to argan oil. *Food Chem.* **2015**, *181*, 270–276. [CrossRef] [PubMed]

26. Liu, H.; Liu, Y.J.; Yang, M.F.; Shen, S.H. A comparative analysis of embryo and endosperm proteome from seeds of *Jatropha curcas*. *J. Integr. Plant Biol.* **2009**, *51*, 850–857. [CrossRef] [PubMed]
27. Chen, M.S.; Wang, G.J.; Wang, R.L.; Wang, J.; Song, S.Q.; Xu, Z.F. Analysis of expressed sequence tags from biodiesel plant *Jatropha curcas* embryos at different developmental stages. *Plant Sci.* **2011**, *181*, 696–700. [CrossRef] [PubMed]
28. Lopes, M.A.; Larkins, B.A. Endosperm origin, development, and function. *Plant Cell* **1993**, *5*, 1383–1399. [CrossRef] [PubMed]
29. Liu, H.; Yang, Z.; Yang, M.; Shen, S. The differential proteome of endosperm and embryo from mature seed of *Jatropha curcas*. *Plant Sci.* **2011**, *181*, 660–666. [CrossRef] [PubMed]
30. Brink, R.A.; Cooper, D.C. The endosperm in seed development. *Bot. Rev.* **1947**, *13*, 479–541. [CrossRef]
31. Cao, H.; He, M.; Zhu, C.; Yuan, L.; Dong, L.; Bian, Y.; Zhang, W.; Yan, Y. Distinct metabolic changes between wheat embryo and endosperm during grain development revealed by 2D-DIGE-based integrative proteome analysis. *Proteomics* **2016**, *16*, 1515–1536. [CrossRef] [PubMed]
32. Severino, L.S.; Mendes, B.S.; Lima, G.S. Seed coat specific weight and endosperm composition define the oil content of castor seed. *Ind. Crop. Prod.* **2015**, *75*, 14–19. [CrossRef]
33. Ohlrogge, J.B.; Jaworski, J.G. Regulation of fatty acid synthesis. *Annu. Rev. Plant Biol.* **1997**, *48*, 109–136. [CrossRef] [PubMed]
34. Weselake, R.J.; Byers, S.D.; Davoren, J.M.; Laroche, A.; Hodges, D.M.; Pomeroy, M.K.; Furukawa-Stoffer, T.L. Triacylglycerol biosynthesis and gene expression in microspore-derived cell suspension cultures of oilseed rape. *J. Exp. Bot.* **1998**, *49*, 33–39. [CrossRef]
35. Lardizabal, K.; Effertz, R.; Levering, C.; Mai, J.; Pedroso, M.C.; Jury, T.; Aasen, E.; Gruys, K.; Bennett, K. Expression of *Umbelopsis ramanniana DGAT2A* in seed increases oil in soybean. *Plant Physiol.* **2008**, *148*, 89–96. [CrossRef] [PubMed]
36. Chen, J.M.; Qi, W.C.; Wang, S.Y.; Guan, R.Z.; Zhang, H.S. Correlation of Kennedy pathway efficiency with seed oil content of canola (*Brassica napus* L.) lines. *Can. J. Plant Sci.* **2011**, *91*, 251–259. [CrossRef]